IOP Publishing New J. Phys. 26 (2024) 013003 https://doi.org/10.1088/1367-2630/ad153b

New Journal of Physics
The open access journal at the forefront of physics

Deutsche Physikalische Gesellschaft DPG
IOP Institute of Physics

Published in partnership with: Deutsche Physikalische Gesellschaft and the Institute of Physics

OPEN ACCESS

RECEIVED
26 September 2023

REVISED
6 December 2023

ACCEPTED FOR PUBLICATION
13 December 2023

PUBLISHED
5 January 2024

PAPER

Coherent anharmonicity transfer from matter to light in the THz regime

Mauricio Arias[1], **Johan F Triana**[2], **Aldo Delgado**[1,3] and **Felipe Herrera**[3,4,*]

[1] Departament of Physics, Facultad de Ciencias Físicas y Matemáticas, Universidad de Concepción, Concepción, Chile
[2] Departament of Physics, Universidad Católica del Norte, Av. Angamos 0610, Antofagasta, Chile
[3] ANID-Millennium Institute for Research in Optics, Concepción, Chile
[4] Departament of Physics, Universidad de Santiago de Chile, Av. Victor Jara 3493, Santiago, Chile
[*] Author to whom any correspondence should be addressed.

E-mail: felipe.herrera.u@usach.cl

Keywords: quantum wells, non-linear phase, light–matter interaction, coherent transfer, cavity-QED

Abstract

Optical nonlinearities are fundamental in several types of optical information processing protocols. However, the high laser intensities needed for implementing phase nonlinearities using conventional optical materials represent a challenge for nonlinear optics in the few-photon regime. We introduce an infrared cavity quantum electrodynamics (QED) approach for imprinting nonlinear phase shifts on individual THz pulses in reflection setups, conditional on the input power. Power-dependent phase shifts on the order of $0.1\,\pi$ can be achieved with femtosecond pulses of only a few μW input power. The proposed scheme involves a small number of intersubband quantum well transition dipoles evanescently coupled to the near field of an infrared resonator. The field evolution is nonlinear due to the dynamical transfer of spectral anharmonicity from material dipoles to the infrared vacuum, through an effective dipolar chirping mechanism that transiently detunes the quantum well transitions from the vacuum field, leading to photon blockade. We develop analytical theory that describes the dependence of the imprinted nonlinear phase shift on relevant physical parameters. For a pair of quantum well dipoles, the phase control scheme is shown to be robust with respect to inhomogeneities in the dipole transition frequencies and relaxation rates. Numerical results based on the Lindblad quantum master equation validate the theory in the regime where the material dipoles are populated up to the second excitation manifold. In contrast with conventional QED schemes for phase control that require strong light–matter interaction, the proposed phase nonlinearity works best in weak coupling, increasing the prospects for its experimental realization using current nanophotonic technology.

1. Introduction

Cavity quantum electrodynamics (QED) is one of the building blocks of quantum technology [1, 2]. Strong light–matter interaction between dipolar material resonances and the electromagnetic vacuum of a cavity has been used for protecting and manipulating quantum information across the entire frequency spectrum using neutral atoms [3, 4], semiconductors [5–8], and superconducting artificial atoms [9–13]. Cavity QED observables such as the vacuum Rabi splitting have also been demonstrated with material dipoles in infrared (THz) resonators at room temperature using intersubband transitions [14–17] and molecular vibrations [18–23], for applications such as infrared photodetection [24] and controlled chemistry [25, 26]. The enhancement of the spontaneous emission rate of material dipoles in a weakly coupled cavity via the Purcell effect [27–29] has been used over different frequency regimes for reservoir engineering [30, 31], dipole cooling [32, 33] and quantum state preparation [34]. In infrared cavities, the Purcell effect can be an effective tool for studying the relaxation dynamics of THz transitions in materials [35–37], given the negligible radioactive decay rates at these frequencies in comparison with non-radioactive relaxation processes [38, 39]. The direct linear measurement of confined infrared field dynamics in a weakly coupled dipole-cavity system

[40] can thus provide information about infrared transitions that otherwise would only be accessible using ultrasfast nonlinear spectroscopy [41, 42].

Cavity QED also enables the manipulation of external electromagnetic fields that drive a coupled cavity-dipole system [5]. Implementing conditional phase shifts via intracavity light–matter interaction can be used for quantum information processing [43–45], as demonstrated using atomic dipoles [46, 47] and quantum dots [48, 49] in optical cavities. In analogy with classical phase modulation processes in bulk nonlinear optical materials [50], which depend on the anharmonic response of the medium to strong fields [51], cavity-assisted phase shifts are possible due to photon blockade effects that arise due to intrinsic spectral anharmonicities of strongly coupled light-matter systems [52, 53]. In the infrared regime, despite the growing interest in cavity QED phenomena with molecular vibrations [25, 26, 40, 54–59] and semiconductors [16, 60–62], viable physical mechanisms for implementing conditional phase dynamics with infrared fields have yet to be developed.

Here we study a previously unexplored form of dynamical photon blockade effect that can be used for imprinting intensity-dependent phase shifts on electromagnetic pulses at THz frequencies (mid-infrared). The physical mechanism that supports the phase nonlinearity involves an effective transfer of the spectral anharmonicity of suitable few-level systems to the near field of an infrared resonator in weak coupling. To emphasize the feasibility of implementing the proposed phase nonlinearity using current technology, the relevant frequency scales of the problem are specified according to recent cavity QED experiments with intersubband transitions of multi quantum wells (MQWs) embedded in infrared nanoresonators [16]. The proposed scheme should be simpler with MQW than ensembles of molecular vibrations [36], because the number of dipoles is much smaller and the spectral anharmonicity much higher. By driving the resonator with a moderately strong femtosecond laser pulse, the matter-induced phase nonlinearity can be retrieved from the free-induction decay (FID) of the resonator near field $E_{\rm nf}(t)$ using linear heterodyne spectroscopy techniques with femtosecond time resolution [35, 37, 63–67].

The article is organized as follows: section 2 describes the model for a MQW coupled to a common open cavity field. Section 3 develops a mean-field theory of the dynamical chirping effect that gives rise to the infrared phase nonlinearity. Section 4 discusses the scaling of the predicted nonlinear phase shift with the physical parameters of the problem for identical intersubband dipoles. Section 5 shows that the results are robust with respect to dipole inhomogeneities. Numerical validation of the theory is given in section 6 using a Lindblad quantum master equation description of the system dynamics. We summarize and discuss perspectives of this work in the Conclusions.

2. Cavity QED model of anharmonic semiconductor dipoles

We consider a small number N of quantum wells located within the near field of a resonant infrared nanoantenna, as illustrated in figure 1. The quantum wells do not interact with each other and have discrete intersubband energy levels with transition frequencies in the THz regime [68]. The bare Hamiltonian of the MQW system is a collection of anharmonic quantum Kerr oscillators ($\hbar \equiv 1$ throughout)

$$\hat{H}_n = \omega_n \hat{b}_n^\dagger \hat{b}_n - U_n \hat{b}_n^\dagger \hat{b}_n^\dagger \hat{b}_n \hat{b}_n, \tag{1}$$

where $\hat{b}_n$ is the annihilation operator of the nth quantum well dipole, ω_n is the fundamental frequency and U_n the anharmonicity parameter. The geometry of the quantum well structure determines the confined charge carriers potential and the spectral anharmonicity [69].

Projecting into a complete eigenbasis $|\nu_n\rangle$, equation (1) can be written as $\hat{H}_n = \sum_\nu E_{\nu_n} |\nu_n\rangle\langle\nu_n|$, with eigenvalues $E_{\nu_n} = \omega_n \nu_n - U_n(\nu_n^2 - \nu_n)$. The energy difference between consecutive levels of the nth quantum well is $E_{\nu+1} - E_\nu = \omega_n - 2U_n\nu$. The nonlinear parameter U_n thus lowers the energy spacing of the $1 \to 2$ excitation by $\Delta = 2U_n$ relative to the fundamental frequency. In comparison with molecular vibrations, for which $\Delta \sim 10 - 40\ \mathrm{cm}^{-1}$ [70, 71], multi-quantum well dipoles enable much larger anharmonicities, with $U_n \sim 100 - 300\ \mathrm{cm}^{-1}$ [16].

The anharmonic quantum wells couple to a common resonator near field $\hat{a}$ in the rotating wave approximation are described by the Hamiltonian

$$\hat{\mathcal{H}} = \omega_c \hat{a}^\dagger \hat{a} + \sum_{n=1}^{N} \left[\hat{H}_n + g_n \left(\hat{a}\hat{b}_n^\dagger + \hat{a}^\dagger \hat{b}_n \right) \right], \tag{2}$$

where ω_c is the resonant field mode frequency and $g_n = \mathcal{E}_0 d_n$ is the light-matter coupling strength. The latter depends on the square-root amplitude of the vacuum fluctuations $\mathcal{E}_0$ and the transition dipole moment d_n. For simplicity, we assume transition dipoles are state-independent ($d_n = d_0$) but other choices do not qualitatively affect the results.

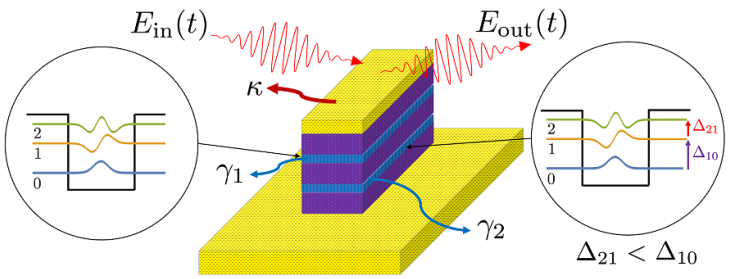

Figure 1. Schematic picture of a MQW in a driven open infrared nanocavity. Two quantum wells forming a MQW with fundamental frequency $\omega_0 = \Delta_{10}$. The $0 \rightarrow 1$ and $1 \rightarrow 2$ transitions are coupled to the near-field of an open nanocavity with frequency ω_c. The coupled light-matter system is driven by an incoming laser pulse with field profile $E_{\rm in}(t)$. The photons that leak out the nanocavity on sub-picosecond time scales at rate κ generate the free-induction decay (FID) signal encoded in the outgoing field $E_{\rm out}(t)$.

We calculate the dissipative dynamics of the system in the presence of a driving pulse according to the Lindblad quantum master equation

$$\frac{\mathrm{d}}{\mathrm{d}t}\hat{\rho} = -i\left[\hat{\mathcal{H}} + \hat{H}_{\rm d}(t), \hat{\rho}\right] + \mathcal{L}_{\kappa}[\hat{\rho}] + \mathcal{L}_{\gamma}[\hat{\rho}], \tag{3}$$

where $\hat{\rho}$ is the density matrix of the total cavity-MQW system. $\mathcal{L}_{\kappa}[\hat{\rho}]$ and $\mathcal{L}_{\gamma}[\hat{\rho}]$ are photonic and material relaxation superoperators given by

$$\mathcal{L}_{\kappa}[\hat{\rho}] = \frac{\kappa}{2}\left(2\hat{a}\hat{\rho}\hat{a}^{\dagger} - \hat{a}^{\dagger}\hat{a}\hat{\rho} - \hat{\rho}\hat{a}^{\dagger}\hat{a}\right), \tag{4}$$

$$\mathcal{L}_{\gamma}[\hat{\rho}] = \sum_{n=1}^{N}\frac{\gamma_n}{2}\left(2\hat{b}_n\hat{\rho}\hat{b}_n^{\dagger} - \hat{b}_n^{\dagger}\hat{b}_n\hat{\rho} - \hat{\rho}\hat{b}_n^{\dagger}\hat{b}_n\right), \tag{5}$$

where κ and γ_n are the decay rates of photonic and nth quantum well modes, respectively. The decoherence processes encoded in γ_n are mainly given by the interaction between MQW and the thermalized phonon bath of the semiconductor structure [72]. For the open cavity field, the main source of decoherence is non radioactive decay in the metal [73], as well as radioactive losses. In this work, the light-matter system is considered to be in the weak coupling regime, broadly defined by the absence of vacuum Rabi splitting in linear transmission [36], which results from a small cooperativity parameter $Ng^2/\kappa\gamma < 1$. The time-dependent Hamiltonian $\hat{H}_{\rm d}(t)$ that describes the driving pulse is given by

$$\hat{H}_{\rm d}(t) = F_0\varphi(t)\left(\hat{a}e^{i\omega_{\rm d}t} + \hat{a}^{\dagger}e^{-i\omega_{\rm d}t}\right), \tag{6}$$

with the Gaussian pulse envelope $\varphi(t) = \exp[-(t-t_0)^2/(2T^2)]$ and carrier frequency $\omega_{\rm d}$. $|F_0|^2$ is proportional to the incoming photon flux[5], t_0 is the pulse center time and T is the pulse duration.

3. Mean-field nonlinear chirping model

We assume that the system dynamics involves only the lowest three energy levels of the quantum wells (i.e. $\nu_{\rm max} = 2$). To ensure that higher energy levels do not contribute significantly to the system evolution, we assume the driving condition $F_0/\kappa < 1$, which is not necessarily weak driving in the sense that the coupled system response can still be nonlinear, but the photon occupation in the near field remains below unity on average. Mean-field equations of motion for identical quantum wells can be obtained from equation (3) for light and matter coherences, to give coupled non-linear system

$$\frac{\mathrm{d}}{\mathrm{d}t}\langle\hat{a}\rangle = -\left(\frac{\kappa}{2} + i\omega_{\rm c}\right)\langle\hat{a}\rangle - i\sqrt{N}g\langle\hat{B}_0\rangle - i\tilde{F}_{\rm d}(t) \tag{7}$$

$$\frac{\mathrm{d}}{\mathrm{d}t}\langle\hat{B}_0\rangle = -\left[\frac{\gamma}{2} + i\left(\omega_0 - \frac{2U}{N}|\langle\hat{B}_0\rangle|^2\right)\right]\langle\hat{B}_0\rangle - i\sqrt{N}g\langle\hat{a}\rangle, \tag{8}$$

where $\hat{B}_0 = (1/\sqrt{N})\sum_n \hat{b}_n$ is the bright collective oscillator mode of fundamental frequency ω_0 and decay rate γ. The driving parameter is $\tilde{F}_{\rm d} = F_0\varphi(t)\exp(-i\omega_{\rm d}t)$. For simplicity we consider that all quantum wells

[5] The stationary photon flux in the continuous wave regime of an empty cavity with radiative decay rate κ is $\Phi_{\rm flux} = \kappa\langle\hat{a}^{\dagger}\hat{a}\rangle = 4|F_0|^2/\kappa$.

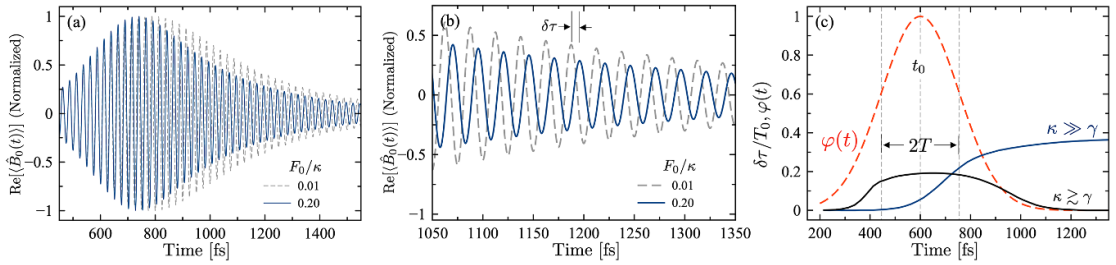

Figure 2. Dipolar FID signals. (a) Real part of the material collective coherence $\mathrm{Re}\langle\hat{B}_0(t)\rangle$ for two identical quantum wells coupled to a common field mode. The antenna is driven by a laser pulse with carrier frequency ω_d, pulse duration $T = 155$ fs, centered at $t_0 = 600$ fs. Pulse strength parameters $F_0 = 0.01\kappa$ and $F_0 = 0.20\kappa$ are assumed. Additional parameters are $\{\omega_0, \kappa, \gamma, U, \sqrt{N}g\} = \{40.0, 12.0, 0.6, 0.6, 1.0\}$ THz. (b) Zoom of the FID signals shown in (a) to visualize the time delay $\delta\tau$ generated after the pulse is over. (c) Time delay ratio calculated as the time difference between peaks of the material collective coherence, for $\gamma = 0.6$ THz (blue curve, different material and nanocavity bandwidths) and $\gamma = 10.0$ THz (black curve, comparable bandwidths). The dashed red line shows the Gaussian pulse profile.

are equally coupled to the field mode and have the same anharmonicity, by setting $g_n = g$ and $U_n = U$. For homogeneous systems, the $N-1$ dark collective modes $\hat{B}_\alpha = (1/\sqrt{N})\sum_n c_{\alpha,n}\hat{b}_n$, with $c_{\alpha,n} = \exp(i2\alpha n/N)$, evolve completely decoupled from equations (7) and (8) (see appendix A). The Kerr nonlinearity generates an effective dipole chirping effect, with instantaneous frequency

$$\omega_0'(t) = \omega_0 - \frac{2U}{N}|\langle\hat{B}_0(t)\rangle|^2. \tag{9}$$

This is red shifted from the fundamental resonance by an amount proportional to the bright mode occupation. The nonlinearity is proportional to the anharmonicity parameter U and is small for large N [36]. The transient red shift occurs while the system is driven by the laser pulse, which populates $\hat{B}_0(t)$, and is thus proportional to the photon flux parameter F_0.

We solve equations (7) and (8) analytically to gain insight on the chirping effect. We assume that the bandwidth of the dipole resonance is much smaller than the antenna bandwidth, i.e. we work in the weak coupling regime, where $\kappa \gg \gamma$ and $4Ng^2/\kappa\gamma < 1$. By adiabaticaly eliminating the antenna field from the dynamics, the evolution of bright mode after the pulse is over is given by

$$\langle\hat{B}_0(t)\rangle = B_{\mathrm{off}} e^{-\frac{\tilde{\gamma}}{2}(t-t_{\mathrm{off}})} e^{i\phi(t)} \tag{10}$$

where t_{off} is the pulse turn-off time. The phase evolves as

$$\phi(t) = \phi_{\mathrm{off}} + \frac{2UB_{\mathrm{off}}^2}{N\tilde{\gamma}}\left\{1 - e^{-\tilde{\gamma}(t-t_{\mathrm{off}})}\right\}, \tag{11}$$

where $\tilde{\gamma} = \gamma(1 + 4Ng^2/\kappa\gamma)$ is the Purcell-enhanced dipole decay rate [37, 74] and $B_{\mathrm{off}} = |\langle\hat{B}_0(t_{\mathrm{off}})\rangle|$. Defining $\tau = t - t_{\mathrm{off}}$, in the long time regime, $\tau\tilde{\gamma} \gg 1$, equation (11) gives the stationary relative phase

$$\Delta\phi_{\mathrm{ss}} = \phi_{\mathrm{ss}} - \phi_{\mathrm{off}} = \frac{2UB_{\mathrm{off}}^2}{N\tilde{\gamma}}, \tag{12}$$

which depends quadratically on the laser strength, through the implicit linear dependence of B_{off} on F_0. The derivation of equation (11) can be found in appendix B. In the limiting cases of harmonic oscillators ($U = 0$), thermodynamic limit ($N \to \infty$), or linear response ($F_0/\kappa \ll 1$), the relative phase is negligible ($\Delta\phi_{\mathrm{ss}} \approx 0$). Molecular ensembles have low anharmonicites, and have been shown to require higher pulse strengths to produce finite relative phases [36] than the ones discussed here.

Figures 2(a) and (b) show the evolution of the dipole coherence $\mathrm{Re}[\langle\hat{B}_0(t)\rangle]$ obtained by solving equations (7)–(8) numerically with parameters relevant for experimental implementations [16, 69]. Figure 2(b) shows the time delay $\delta\tau$ produced by a strong driving pulse ($F_0/\kappa = 0.2$) on the FID signal, in comparison with weak pulses. The delay $\delta\tau$ in time domain results in the relative phase from equation (12). Recent experiments with infrared nanoantennas have the femtosecond temporal resolution necessary to measure $\delta\tau$ [36, 37].

Figure 2(c) shows the evolution of $\delta\tau$ for two scenarios. For long dipole lifetimes ($\gamma \ll \kappa$), i.e. narrowband MQW response, the time delay of the FID signal remains after the driving pulse is over. On the contrary, when $\gamma \sim \kappa$ the time delay disappears after the pulse ends. The system thus requires long dipole dephasing times to imprint a stationary time delay in the near field once the driving pulse is turned off.

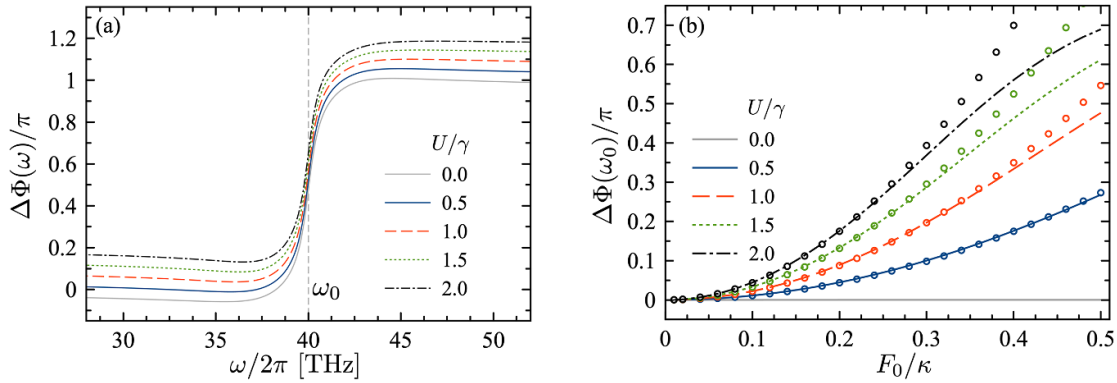

Figure 3. Intensity-dependent phase spectrum of the scattered field. (a) Relative phase spectrum $\Delta\Phi(\omega)$ for $F_0 = 0.2\kappa$ and different values of U/γ. (b) Nonlinear phase spectrum $\Delta\Phi(\omega_0)/\pi$ at ω_0 as a function of the laser strength parameter F_0/κ. Circle symbols correspond to an analytical quadratic scaling with fit parameter $\alpha = 3.5$. Both panels are calculated using equation (14) for different ratios U/γ. Additional parameters are $\{\omega_0, \kappa, \gamma, \sqrt{N}g\} = \{40.0, 12.0, 0.6, 1.0\}$ THz.

4. Nonlinear phase shift in the frequency domain

The time delay in the collective material coherence $\langle\hat{B}_0(t)\rangle$ from figure 2 is transferred to the photonic coherence $\langle\hat{a}(t)\rangle$, which ultimately gives the observable FID signal in heterodyne measurements [36, 37]. We define the Fourier transform of the field coherence as

$$\langle\hat{a}(\omega)\rangle = \frac{1}{\sqrt{2\pi}}\int_{-\infty}^{\infty} \mathrm{d}t\langle\hat{a}(t)\rangle e^{i\omega t}, \tag{13}$$

and calculate the phase response $\Phi(\omega)$ of the FID signal as

$$\Phi(\omega) = \arctan\left(\frac{\mathrm{Im}[\langle\hat{a}(\omega)\rangle]}{\mathrm{Re}[\langle\hat{a}(\omega)\rangle]}\right). \tag{14}$$

The Fourier transform is taken for the post-pulse FID signal. Figure 3(a) shows the phase spectrum for different values of the parameter U/γ, at fixed driving strength ($F_0 = 0.2\kappa$). The relative phase in Fourier space is negligible for the limiting cases discussed above. In the case of anharmonic MQWs, the relative phase $\Delta\Phi(\omega) = \Phi(\omega) - \Phi_{\mathrm{harm}}$ increases as the anharmonicity parameter U/γ grows for fixed F_0, with Φ_{harm} given by relative phase obtained under harmonic conditions.

To gain insight on the behavior of the relative nonlinear phase, we use equation (10) to calculate $\Delta\Phi(\omega)$ analytically in the Fourier domain. We obtain

$$\Delta\Phi(\omega_0) = \alpha\frac{2U}{N\tilde{\gamma}}\left(\frac{F_0}{\kappa}\right)^2, \tag{15}$$

where the numerical parameter α comes from the proportionality relation $|\langle\hat{B}_0(t)\rangle| \propto F_0$ and the fact that ϕ_{off} in equation (11) is also a nonlinear phase that grows with the dipole amplitude before the driving pulse is off. The derivation of equation (15) and additional details can be found in appendix B. Figure 3(b) shows the analytical fitting and numerical calculations for the nonlinear phase shift at the fundamental frequency ω_0 as a function of the laser intensity parameter F_0/κ, for different values of U/γ. In agreement with previous works [75, 76], in the weak driving limit ($F_0/\kappa \ll 1$) we obtain the linear response regime, i.e. $\Delta\Phi(\omega_0) \approx 0$ from equation (15), which is also demonstrated numerically in figure 3(b). In the low anharmonicity regime $U/\gamma < 1$, the nonlinear phase has a clear quadratic dependence on F_0, while for strong anharmonicities $U/\gamma \gtrsim 1$, $\Delta\Phi(\omega_0)$ is quadratic for only up to a certain driving strength. Beyond this point, higher energy levels ($\nu > 2$) start to contribute with the dynamics of the system and the adiabatic elimination approach used to derive equation (15) breaks down.

5. Nonlinear phase shift enhancement via dark states

The dynamics in the totally symmetric case with identical QW dipoles only involves the field and bright collective modes without the influence of the dark manifold. For a pair of inhomogeneous QWs ($N = 2$), the equation of motion for the bright mode $\langle\hat{B}_0\rangle$ should be extended to read

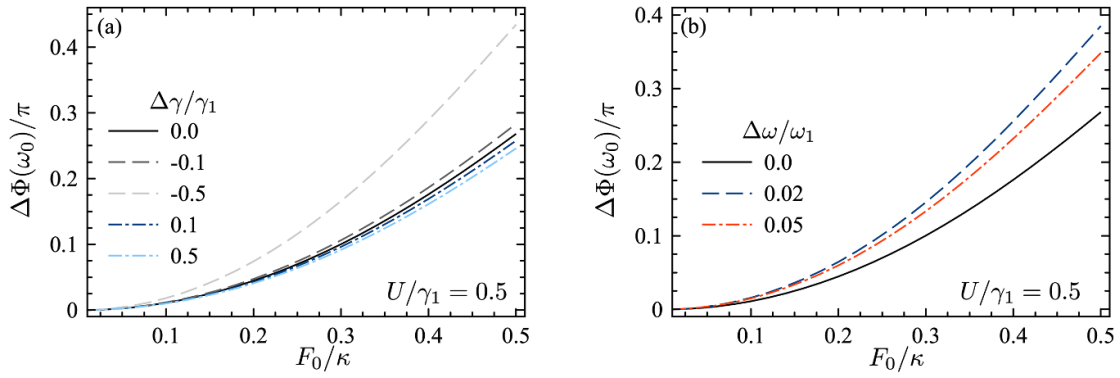

Figure 4. Nonlinear phase shift enhancement via dipole inhomogeneity. Nonlinear phase shift at ω_0 as a function of the driving ratio F_0/κ for the anharmonicity parameter $U/\gamma_1 = 0.5$. (a) For $\omega_1 = \omega_2 = \omega_0$ and $\gamma_1 \neq \gamma_2$. (b) For $\omega_0 = \omega_1 \neq \omega_2$ and $\gamma_1 = \gamma_2$. Additional parameters are $\{\omega_0, \kappa, \gamma_1, \sqrt{N}g\} = \{40.0, 12.0, 0.6, 1.0\}$ THz.

$$\frac{\mathrm{d}}{\mathrm{d}t}\langle\hat{B}_0\rangle = -\left(\frac{\bar{\gamma}}{2} + i\bar{\omega}\,(t)\right)\langle\hat{B}_0\rangle - \left(\frac{\Delta\gamma}{2} + i\Delta\omega\,(t)\right)\langle\hat{B}_1\rangle - i\sqrt{N}g\langle\hat{a}\rangle \tag{16}$$

where $\langle\hat{B}_1\rangle = (-\langle\hat{b}_1\rangle + \langle\hat{b}_2\rangle)/\sqrt{2}$ is the dark mode for the pair of dipoles, $\bar{\gamma} = (\gamma_1 + \gamma_2)/2$ and $\Delta\gamma = (\gamma_2 - \gamma_1)/2$ are the average value and the mismatch of decay rates, respectively. The instantaneous average frequency is now given by

$$\bar{\omega}\,(t) = \bar{\omega} - U\left(|\langle\hat{B}_0\,(t)\rangle|^2 + |\langle\hat{B}_1\,(t)\rangle|^2\right) \tag{17}$$

and the frequency mismatch by

$$\Delta\omega\,(t) = \Delta\omega - 2U\mathrm{Re}\left[\langle\hat{B}_0\,(t)\rangle^*\langle\hat{B}_1\,(t)\rangle\right], \tag{18}$$

where $\bar{\omega} = (\omega_1 + \omega_2)/2$ and $\Delta\omega = (\omega_2 - \omega_1)/2$. The coupling of the dark mode $\langle\hat{B}_1\rangle$ with the bright mode influences the dynamics of the system. It is clear that in the totally symmetric case ($\Delta\gamma = \Delta\omega = 0$), bright and dark modes are decoupled and equation (16) reduces to equation (8). The positive additive contribution $|\langle\hat{B}_1\rangle|^2$ to the instantaneous dipole frequency suggests that the dark manifold enhances the nonlinear phase shift. The derivation of equation (16) can be found in appendix C.

Figure 4 shows the nonlinear phase spectrum of $\langle\hat{a}(\omega)\rangle$ evaluated at the fundamental frequency ω_0 for two inhomogeneus scenarios. First, we set equal fundamental frequencies with variations in the decay rates of the QWs, i.e. $\omega_1 = \omega_2 = \omega_0$ and $\gamma_1 \neq \gamma_2$. In figure 4(a) we find both enhancement and reduction of the nonlinear phase for $U = 0.5\gamma_1$. Enhancement is reached for $\Delta\gamma < 0$, which is due to a reduction of the effective decay rate $\bar{\gamma}$ associated with bright mode in equation (16). In the opposite case, i.e. for $\gamma_2 > \gamma_1$, $\Delta\Phi(\omega_0)$ decreases due to the increased decay rate of the bright mode. The second scenario considers one QW detuned with respect to the other but both having equal decay rates, i.e. $\omega_1 \neq \omega_2$ and $\gamma_1 = \gamma_2$. The results are shown in figure 4(b). In this case, the small blue and red detuning of one of the quantum wells gives a nonlinear phase enhancement. However, for very large detunings ($\Delta\omega/\omega_0 > 0.1$) the nonlinear phase tends to the homogeneous limit ($\Delta\omega = 0$), as the detuned quantum well becomes effectively decoupled from the field.

6. Validity of the mean-field theory

We calculate the evolution of the total density matrix by solving the Lindblad quantum master equation in equation (3) by using *QuTiP* [77, 78] to explore the regime of validity of the mean-field theory for a pair of anharmonic quantum well dipoles. The evolution of the density matrix converges with a truncated Hilbert space that includes up to $\nu_{\max} = 4$ intersubband excitations per quantum well and $n_{\max} = 5$ photons, which results in a Hilbert space dimension of $d = 150$.

Figures 5(a) and (b) show the nonlinear phase shift $\Delta\Phi(\omega_0)$ as a function of the laser strength parameter F_0/κ predicted by the Lindblad QME for two different values of the anharmonicity: $U = 0.5\gamma_1$ and

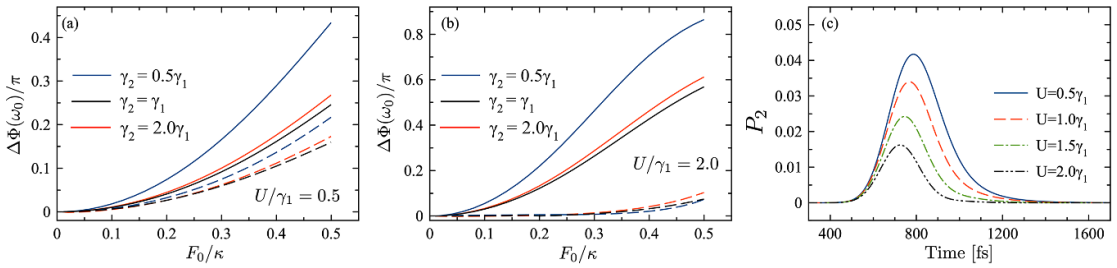

Figure 5. Fully quantum validation of the nonlinear phase shift. Relative nonlinear phase shift as a function of laser strength parameter F_0/κ found in the mean-field approximation (solid lines) and by solving the Lindblad quantum master equation (dashed lines) for different inhomogeneous scenarios and for (a) $U/\gamma_1 = 0.5$ and (b) $U/\gamma_1 = 2.0$. (c) Population dynamics of the second excited energy level P_2 for $F_0 = 0.3\kappa$ and different values of the anharmonicity parameter U/γ_1. Additional parameters for all panels are $\{\omega_0, \kappa, \gamma_1, \sqrt{N}g\} = \{40.0, 12.0, 0.6, 1.0\}$ THz. The mean-field approximation and the Lindblad quantum master are implemented with the same parameters.

$U = 2.0\gamma_1$. For $U = 0.5\gamma_1$, both mean-field (solid lines) and fully quantum (dashed lines) calculations agree up to a factor of two approximately (see additional comparisons in appendix D). However, $\Delta\Phi(\omega_0)$ in the mean-field approach is overestimated for $U = 2.0\gamma_1$, where the nonlinear phase is negligible up to $F_0/\kappa \approx 0.4$, then increases for higher laser intensities. The latter is due to the large detuning between cavity frequency ω_c and Δ_{21}. As a consequence, anharmonic blockade is observed for the intersubband state $\nu = 2$ such that the higher level does not participate in the dynamics, causing the dipole to behave effectively as a harmonic oscillator. In figure 5(c), we show the population of the $\nu = 2$ level (P_2) for $F_0/\kappa = 0.3$ and different values of the anharmonicity parameter U/γ_1. P_2 is suppressed as U increases due to the blockade effect [52, 53, 79]. The mean-field theory is accurate for weak pulses ($F_0/\kappa < 0.1$) independent on the anharmonicity parameter U/γ and, for stronger pulses with anharmonicities lower than dissipation rate of MQWs ($U/\gamma < 1.0$).

7. Discussion and conclusion

In this work, we described a novel dynamical photon blockade mechanism in THz cavity QED that can be used for imprinting power-dependent phase shifts on the electromagnetic response of a coupled cavity-dipole system. We develop analytical quantum mechanical theory to model FID signals of a pulse-driven cavity system, using parameters that are relevant for quantum well intersubband transitions in mid-infrared resonators [16]. For N quantum wells within the near field of the driven resonator, the theory shows that using only a moderately strong pulse that drives a small fraction of the intersubband level population to the second excitation manifold, a stationary phase shift proportional to the spectral anharmonicity parameter $U/N\gamma$ and the photon flux of the pulse, can be imprinted on the FID response of the near field, which can then be retrieved using time-domain spectroscopic techniques [40]. We point out that the relative phase shift is unaffected if excited energy levels higher than $\nu > 2$ are populated, which occurs by driving the resonator with laser pulses strengths higher than $F_0/\kappa > 0.5$. For experimentally relevant system parameters [16], with photon flux Φ_{flux} in the stationary regime and setting $F_0 = 0.5\kappa$, nonlinear phase shifts of order of 1 radian are predicted for a single quantum well using a single sub-picosecond pulse of a few μW.

The predicted phase nonlinearity can be physically understood as a result of laser-induced dipole effect that dynamically detunes the cavity field with respect to the $1 \rightarrow 2$ intersubband transition, caused by population driven between the first and second excited levels of the anharmonic quantum well spectrum. The analytical model is validated numerically using density matrix solutions of the corresponding Lindblad quantum master equation. Notably, the proposed dipole chirping mechanism only occurs for cavity fields that are much shorter lived than the THz dipole resonance (bad cavity limit), as is the case in several nanophotonic setups [16, 37]. Moreover, the phase imprinting scheme works best in the weak coupling regime, contrary to conventional photon blockade effects developed for optical cavity QED, which require strong coupling conditions [53, 80].

Our work demonstrates the feasibility of implementing nonlinear phase operations at THz frequencies using current available nanocavities [16, 37, 40] and contributes to the development of quantum optics in the high-THz regime [69, 80], which can enable fundamental studies of cavity QED[81, 82], material and

molecular spectroscopy [40, 62, 83], and controlled chemistry in confined electromagnetic environments [25, 26]. Extensions of this work to the analysis of THz and infrared pulses with non-classical field statistics [84, 85] could open further possibilities for developing ultrafast quantum information processing at room temperature.

Data availability statement

All data that support the findings of this study are included within the article (and any supplementary files).

Acknowledgment

M A is funded by ANID—Agencia Nacional de Investigación y Desarrollo through the Scholarship Programa Doctorado Becas Chile/2018 No. 21181591. J F T is supported by ANID—Fondecyt Iniciación Grant No. 11230679. F H is funded by ANID—Fondecyt Regular Grant No. 1221420 and the Air Force Office of Scientific Research under Award Number FA9550-22-1-0245. A D is supported by ANID—Fondecyt Grants No. 1231940 and No. 1230586. All authors also thanks support by ANID—Millennium Science Initiative Program ICN17_012.

Appendix A. Mean-field approach for *N* identical dipoles

The density matrix of the light-matter system $\hat{\rho}(t)$ evolves according to the quantum master equation in Lindblad form

$$\frac{\mathrm{d}}{\mathrm{d}t}\hat{\rho} = -i\left[\hat{\mathcal{H}} + \hat{H}_{\mathrm{d}}(t), \hat{\rho}\right] + \mathcal{L}_{\kappa}[\hat{\rho}] + \mathcal{L}_{\gamma}[\hat{\rho}], \tag{A1}$$

where $\hat{\mathcal{H}}$ is the Hamiltonian of the system in equation (2), $\hat{H}_{\mathrm{d}}(t)$ is the time-dependent Hamiltonian of the laser pulse that drives the nanocavity in equation (6) and the Lindblad superoperators are given by [86, 87]

$$\mathcal{L}_{\kappa}[\hat{\rho}] = \frac{\kappa}{2}\left(2\hat{a}\hat{\rho}\hat{a}^{\dagger} - \hat{a}^{\dagger}\hat{a}\hat{\rho} - \hat{\rho}\hat{a}^{\dagger}\hat{a}\right), \tag{A2}$$

$$\mathcal{L}_{\gamma}[\hat{\rho}] = \sum_{n=1}^{N}\frac{\gamma_n}{2}\left(2\hat{b}_n\hat{\rho}\hat{b}_n^{\dagger} - \hat{b}_n^{\dagger}\hat{b}_n\hat{\rho} - \hat{\rho}\hat{b}_n^{\dagger}\hat{b}_n\right), \tag{A3}$$

κ is the resonator field decay rate and γ_n is the MQW relaxation rate into a local reservoir. $\hat{a}$ and $\hat{b}_n$ are the annihilation operators of the field mode and the nth quantum well, respectively.

The local operators can be expressed as a linear combination of the collective modes $\hat{B}_{\alpha}$ as

$$\hat{b}_n = \frac{1}{\sqrt{N}}\sum_{\alpha=0}^{N-1}\exp\left(-\frac{i2\pi\alpha n}{N}\right)\hat{B}_{\alpha}. \tag{A4}$$

Thus, the Lindblad superoperators for the collective modes considering homogeneous MQWs (with $\gamma_n = \gamma$) are given by

$$\mathcal{L}_{\gamma}[\hat{\rho}] = \frac{\gamma}{2}\sum_{\alpha=0}^{N-1}\left(2\hat{B}_{\alpha}\hat{\rho}\hat{B}_{\alpha}^{\dagger} - \left\{\hat{B}_{\alpha}^{\dagger}\hat{B}_{\alpha}, \hat{\rho}\right\}\right), \tag{A5}$$

where $\{\hat{A}, \hat{B}\}$ is the anticommutator between arbitrary operators $\hat{A}$ and $\hat{B}$.

The exact equations of motion for the field and bright collective matter coherences in the Schrödinger picture are given by

$$\frac{\mathrm{d}}{\mathrm{d}t}\langle\hat{a}\rangle = -\left(\frac{\kappa}{2} + i\omega_{\mathrm{c}}\right)\langle\hat{a}\rangle - i\sqrt{N}g\langle\hat{B}_0\rangle - i\tilde{F}_{\mathrm{d}}(t), \tag{A6}$$

$$\frac{\mathrm{d}}{\mathrm{d}t}\langle\hat{B}_0\rangle = -\left(\frac{\gamma}{2}+i\omega_0\right)\langle\hat{B}_0\rangle - i\sqrt{N}g\langle\hat{a}\rangle + i\frac{2U}{N}\sum_{\beta,\eta=0}^{N-1}\langle\hat{B}^\dagger_\beta\hat{B}_{\beta-\eta(\mathrm{mod}N)}\hat{B}_\eta\rangle, \tag{A7}$$

with $\tilde{F}_\mathrm{d}(t) = F_0\varphi(t)e^{-i\omega_\mathrm{d}t}$, $\langle\hat{B}_\alpha\rangle = \sum_n e^{i2\pi\alpha n/N}\mathrm{Tr}[\hat{b}_n\hat{\rho}(t)]/\sqrt{N}$ and $\xi(\mathrm{mod}N)$ is a modular arithmetic for ξ with modulo N, ensuring the cyclicity of the permutation indexes (for example, for $\beta=0$ and $\eta=1$, $0-1(\mathrm{mod}N) = N-1$). We approximate the expansion of the triple operators in equation (A7) by only using the first term, with $\beta=\eta=0$, and factorizing it as $\langle\hat{B}^\dagger_0\hat{B}_0\hat{B}_0\rangle \approx \langle\hat{B}_0\rangle^*\langle\hat{B}_0\rangle\langle\hat{B}_0\rangle$. This fully-factorized ansatz leads to closed equations of motion for the first moments $\langle\hat{a}\rangle$ and $\langle\hat{B}_0\rangle$ that can describe the nonlinear response of the system. We assess the validity of this approximation in section 6 by solving the full quantum master equation numerically. As expected, the mean-field ansatz is only accurate for weak anharmonicity parameters $U/N\gamma$, where higher order moments that are present in the fully quantum calculations do not contribute significantly.

Appendix B. Adiabatic elimination of the antenna dynamics

In the bad cavity limit, we can adiabatically eliminate the dynamics of the single field mode ($\mathrm{d}\langle\hat{a}(t)\rangle/\mathrm{d}t \to 0$) since $\kappa \gg \gamma$ and $(\kappa-\gamma)/4 > \sqrt{N}g$. We reduce the equations of motion to a single equation for bright collective matter coherence $\hat{B}_0$ which contains the influence of the open cavity mode. Hence, equation (A6) in the rotating frame of the cavity frequency ω_c on resonance with fundamental frequency ω_0 reduces to

$$\langle\tilde{a}^\mathrm{ad}(t)\rangle \approx -i\frac{2\sqrt{N}g}{\kappa}\langle\tilde{B}^\mathrm{ad}_0(t)\rangle - i\frac{2}{\kappa}F_\mathrm{d}(t), \tag{B1}$$

and solving for $\langle\hat{B}_0\rangle$

$$\frac{\mathrm{d}}{\mathrm{d}t}\langle\tilde{B}^\mathrm{ad}_0(t)\rangle = -\frac{\tilde{\gamma}}{2}\langle\tilde{B}^\mathrm{ad}_0(t)\rangle - \frac{2\sqrt{N}g}{\kappa}F_\mathrm{d}(t) + i\frac{2U}{N}|\langle\tilde{B}^\mathrm{ad}_0(t)\rangle|^2\langle\tilde{B}^\mathrm{ad}_0(t)\rangle, \tag{B2}$$

with the renormalized decay rate of the dipole coherence $\tilde{\gamma} = \gamma(1+4Ng^2/\kappa\gamma)$, which is commonly known as the Purcell factor [36].

Equation (B2) with $F_\mathrm{d}(t)=0$ is known in non-linear hydrodynamics as the Stuart-Landau oscillator equation [88, 89]. The laser pulse at a given time $t=t_\mathrm{off}$ turns off and equation (B2) can be solved analytically by a slow variation of the dipole coherence in polar form as $\langle\tilde{B}^\mathrm{ad}_0(t)\rangle = |\langle\tilde{B}^\mathrm{ad}_0(t)\rangle|e^{i\phi(t)}$. Thus, the equations of motion for the amplitude and phase can be written as

$$\frac{\mathrm{d}}{\mathrm{d}t}|\langle\tilde{B}^\mathrm{ad}_0(t)\rangle| = -\frac{\tilde{\gamma}}{2}|\langle\tilde{B}^\mathrm{ad}_0(t)\rangle| \tag{B3}$$

$$\frac{\mathrm{d}}{\mathrm{d}t}\phi(t) = 2\frac{U}{N}|\langle\tilde{B}^\mathrm{ad}_0(t)\rangle|^2, \tag{B4}$$

where their corresponding solutions are given by

$$|\langle\tilde{B}^\mathrm{ad}_0(t)\rangle| = B_\mathrm{off}e^{-\frac{\tilde{\gamma}}{2}(t-t_\mathrm{off})} \tag{B5}$$

$$\phi(t) = \phi_\mathrm{off} + \frac{2UB^2_\mathrm{off}}{N\tilde{\gamma}}\left\{1-e^{-\tilde{\gamma}(t-t_\mathrm{off})}\right\}, \tag{B6}$$

with $B_\mathrm{off} = |\langle\tilde{B}^\mathrm{ad}_0(t_\mathrm{off})\rangle|$ and $\phi_\mathrm{off} = \phi(t_\mathrm{off})$. The dipole coherence in the rotating frame of the laser evolves as

$$\langle\hat{B}^\mathrm{ad}_0(t)\rangle = \langle\hat{B}^\mathrm{ad}_0(t_\mathrm{off})\rangle e^{-\frac{\tilde{\gamma}}{2}(t-t_\mathrm{off})}e^{-i\omega_0(t-t_\mathrm{off})}\exp\left[i\Delta\phi_\mathrm{ss}\left(1-\exp\left[-\tilde{\gamma}\left(t-t_\mathrm{off}\right)\right]\right)\right], \tag{B7}$$

where $\Delta\phi_\mathrm{ss} = \phi_\mathrm{ss} - \phi_\mathrm{off}$ and $\langle\hat{B}^\mathrm{ad}_0(t_\mathrm{off})\rangle = B_\mathrm{off}e^{i\phi_\mathrm{off}}$. The exponential that depends on the relative phase $\Delta\phi$ in equation (B7) evidences the nonlinear contributions, instead of the solution with harmonic MQWs or in the weak driving regime. To clarify, the analogous solution of the dipole coherence with $U=0$ $[\hat{B}^\mathrm{ad}_{0,\mathrm{L}}(t)]$ for $t \geqslant t_\mathrm{off}$ is given by

$$\langle\hat{B}^\mathrm{ad}_{0,\mathrm{L}}(t)\rangle = -\beta(T)\frac{2\sqrt{N}gF_0}{\kappa}e^{-(\tilde{\gamma}/2+i\omega_0)t} \tag{B8}$$

where the factor $\beta(T)$ depends on the envelope functional shape, and the stationary phase $\Delta\phi_{ss} = 0$ due to the system evolves with a constant phase $\phi_{ss} = \phi_{off}$.

In the case of the phase, equation (B6) describes a stationary phase $\phi(t) = \phi_{ss}$ in the long time regime ($t \gg t_{off}$), which is given by

$$\phi_{ss} = \phi_{off} + \frac{2UB_{off}^2}{N\tilde{\gamma}}. \tag{B9}$$

Note that the expression is quadratic respect to amplitude B_{off} and constant for harmonic MQWs ($U = 0$).

B.1. Relation between the dipole and cavity phase shifts

We measure the FID signal in the laboratory, which is related with the field mode coherence $\langle\hat{a}\rangle$. Here, we connect the phase shift that can be obtained from experiments with the phase from the dipole coherence. We define the relative nonlinear phase shift in frequency domain at ω_0 in terms of the Fourier transform of the cavity coherence, $\langle\hat{a}(\omega)\rangle = \mathcal{F}[\langle\hat{a}(t)\rangle](\omega)$, as

$$\Delta\Phi(\omega_0) = \Phi(\omega_0) - \Phi_{harm}(\omega_0), \tag{B10}$$

where,

$$\Phi(\omega) = \arctan\left(\frac{\mathrm{Im}[\langle\hat{a}(\omega)\rangle]}{\mathrm{Re}[\langle\hat{a}(\omega)\rangle]}\right), \tag{B11}$$

and $\Phi_{harm} = \lim_{F_0/\kappa\ll 1}\Phi(\omega_0)$. The latter is valid since the response of the anharmonic dipole oscillator under weak driving conditions $F_0/\kappa \ll 1$ or in the limit of negligible anharmonicity $U/\gamma \to 0$ is equivalent to the linear response, as it is shown in equation (B9). Assuming the same t_{off} for the cavity and dipole coherences, the equations of motion for the field coherence and phase in frequency domain are given by

$$\langle\hat{a}(\omega)\rangle = -i\sqrt{N}g\langle\hat{B}_0(\omega)\rangle\frac{1}{\kappa/2 - i(\omega-\omega_c)}, \tag{B12}$$

$$\Phi(\omega_0) = \Phi^{(0)}(\omega_0) + \arctan\left(\frac{\omega_0-\omega_c}{\kappa/2}\right) - \frac{\pi}{2}, \tag{B13}$$

with

$$\Phi^{(0)}(\omega_0) = \arctan\left(\frac{\mathrm{Im}\left[\langle\hat{B}_0(\omega_0)\rangle\right]}{\mathrm{Re}\left[\langle\hat{B}_0(\omega_0)\rangle\right]}\right).$$

The second and third term in equation (B13) are independent on anharmonicity parameter U/κ and driving strength F_0/κ. Thus, in analogy with equation (B10), i.e. considering that the relative phase shift is given in terms of the linear response and nonlinear contributions, we can write $\Delta\Phi(\omega_0)$ as a function of the dipole coherence instead of the field mode response as

$$\Delta\Phi(\omega_0) = \Delta\Phi^{(0)}(\omega_0) = \Phi^{(0)}(\omega_0) - \Phi^{(0)}_{harm}(\omega_0), \tag{B14}$$

where $\Phi^{(0)}_{harm}(\omega_0) = \lim_{F_0/\kappa\ll 1}\Phi^{(0)}(\omega_0)$.

B.2. Nonlinear phase shift ansatz for an arbitrary driving pulse

We introduce an ansatz for the relative phase since the amplitude $|B_{off}|$ cannot be defined for general driving pulses. We define the nonlinear phase shift $\Delta\Phi$ at frequency ω_0 as

$$\Delta\Phi(\omega_0) = \alpha\frac{2U}{N\tilde{\gamma}}\left(\frac{F_0}{\kappa}\right)^2, \tag{B15}$$

where α is a phenomenological parameter to be explored. The definition in equation (B15) is possible considering that the squared amplitude of the dipole coherence (equation (B5)) and the stationary phase (equation (B9)) grow proportional to the square of the driving strength for the ratio $F_0/\kappa < 1$. Further, numerical results in figure 3 suggest the quadratic dependence.

Appendix C. Mean-field chirping model for asymmetric quantum wells

From the local quantum master equation, the mean-field equations of motion for the coherences of the inhomogeneous quantum wells ($\hat{b}_1$ and $\hat{b}_2$) and field mode $\hat{a}$ are given by

$$\frac{\mathrm{d}}{\mathrm{d}t}\langle\hat{a}\rangle = -\left(\frac{\kappa}{2}+i\omega_\mathrm{c}\right)\langle\hat{a}\rangle - ig\left(\langle\hat{b}_1\rangle+\langle\hat{b}_2\rangle\right) - i\tilde{F}_\mathrm{d}(t), \tag{C1}$$

$$\frac{\mathrm{d}}{\mathrm{d}t}\langle\hat{b}_1\rangle = -\left(\frac{\gamma_1}{2}+i\omega_1\right)\langle\hat{b}_1\rangle - ig\langle\hat{a}\rangle + i2U|\langle\hat{b}_1\rangle|^2\langle\hat{b}_1\rangle, \tag{C2}$$

$$\frac{\mathrm{d}}{\mathrm{d}t}\langle\hat{b}_2\rangle = -\left(\frac{\gamma_2}{2}+i\omega_2\right)\langle\hat{b}_2\rangle - ig\langle\hat{a}\rangle + i2U|\langle\hat{b}_2\rangle|^2\langle\hat{b}_2\rangle. \tag{C3}$$

We set equal light-matter coupling strengths $g = g_1 = g_2$ and anharmonicity parameters $U = U_1 = U_2$. By replacing the bright $\hat{B}_0 = (\hat{b}_1+\hat{b}_2)/\sqrt{2}$ and dark $\hat{B}_1 = (-\hat{b}_1+\hat{b}_2)/\sqrt{2}$ modes, we obtain

$$\frac{\mathrm{d}}{\mathrm{d}t}\langle\hat{a}\rangle = -\left(\frac{\kappa}{2}+i\omega_\mathrm{c}\right)\langle\hat{a}\rangle - i\sqrt{N}g\langle\hat{B}_0\rangle - i\tilde{F}_\mathrm{d}(t), \tag{C4}$$

$$\frac{\mathrm{d}}{\mathrm{d}t}\langle\hat{B}_0\rangle = -\left(\frac{\bar{\gamma}}{2}+i\bar{\omega}(t)\right)\langle\hat{B}_0\rangle - \left(\frac{\Delta\gamma}{2}+i\Delta\omega(t)\right)\langle\hat{B}_1\rangle - i\sqrt{N}g\langle\hat{a}\rangle, \tag{C5}$$

$$\frac{\mathrm{d}}{\mathrm{d}t}\langle\hat{B}_1\rangle = -\left(\frac{\bar{\gamma}}{2}+i\bar{\omega}(t)\right)\langle\hat{B}_1\rangle - \left(\frac{\Delta\gamma}{2}+i\Delta\omega(t)\right)\langle\hat{B}_0\rangle, \tag{C6}$$

with

$$\bar{\omega}(t) = \bar{\omega} - U\left(|\langle\hat{B}_0(t)\rangle|^2 + |\langle\hat{B}_1(t)\rangle|^2\right),$$

and

$$\Delta\omega(t) = \Delta\omega - 2U\mathrm{Re}\left[\langle\hat{B}_0(t)\rangle^*\langle\hat{B}_1(t)\rangle\right],$$

where $\bar{\zeta} = (\zeta_1+\zeta_2)/2$ and $\Delta\zeta = (\zeta_2-\zeta_1)/2$, with $\zeta = \{\gamma,\omega\}$, are the average and mismatch values.

Appendix D. Comparison of mean-field and lindblad quantum master equation

The accuracy of the mean-field results for the nonlinear phase shift $\Delta\Phi_\mathrm{NL}$ in general depends on pulse strength, the degree dipole inhomogeneity and dipole anharmonicity. We assess the parameter dependence of the model predictions in figure D.1, by comparing the predicted nonlinear phase shift as a function of driving strength ratio F_0/κ obtained using the nonlinear mean-field theory and the Lindblad quantum master equation (QME). Results are shown for increasing values of the anharmonicity parameter U/γ_1. Mean-field results coincide well with the QME solution for different values of decay inhomogeneities when both the anharmonicity and driving strengths are not too high ($U/\gamma < 0.4$ and $F_0/\kappa \sim 0.2$). For larger anharmonicity and stronger driving, the nonlinear mean field theory can overestimate the phase shift by a factor of a few.

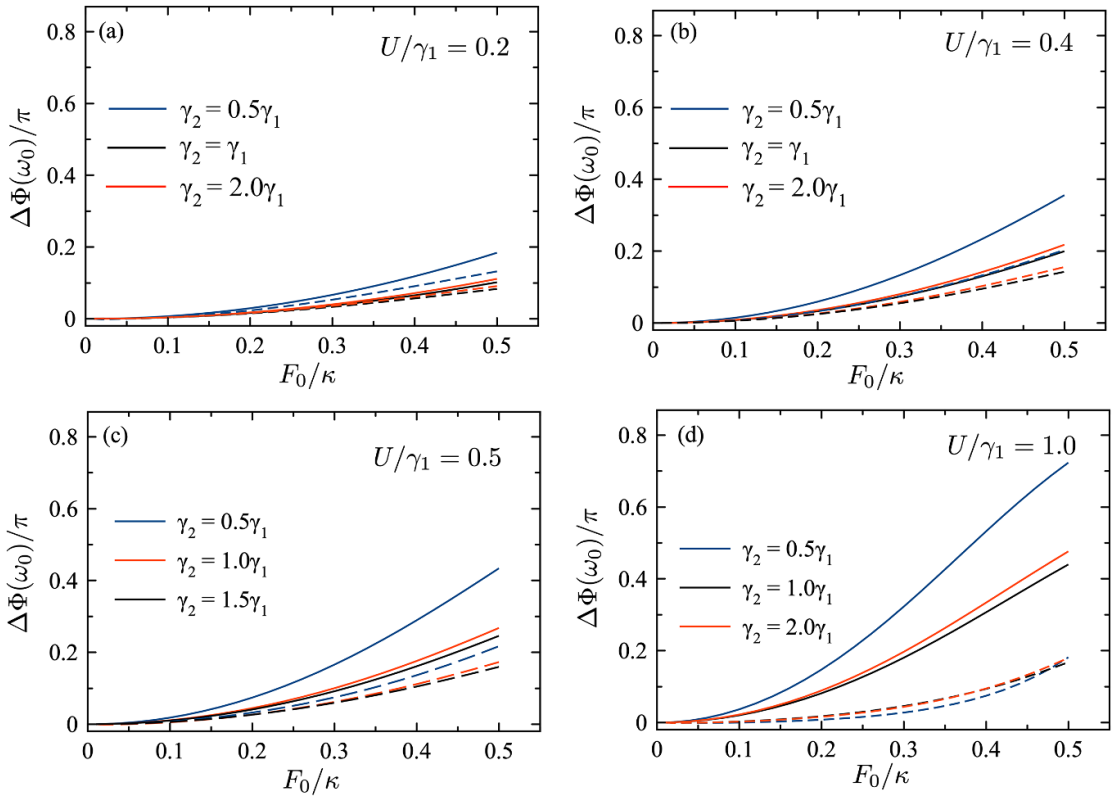

Figure D.1. U—dependent progression of fully quantum validation for the nonlinear phase shift. Relative nonlinear phase shift as a function of laser strength parameter F_0/κ found in the mean-field approximation (solid lines) and by solving the Lindblad quantum master equation (dashed lines) for different inhomogeneous scenarios and for (a) $U/\gamma_1 = 0.2$, (b) $U/\gamma_1 = 0.4$, (c) $U/\gamma_1 = 0.5$ and (d) $U/\gamma_1 = 1.0$. Additional parameters for all panels are $\{\omega_0, \kappa, \gamma_1, \sqrt{N}g\} = \{40.0, 12.0, 0.6, 1.0\}$ THz.

Appendix E. Photon blockade effect

The photon blockade effect can be characterized by the equal-time second-order correlation function

$$g^{(2)}(0) = \frac{\langle \hat{a}^\dagger \hat{a}^\dagger \hat{a}\hat{a} \rangle}{\langle \hat{a}^\dagger \hat{a} \rangle^2}, \tag{E1}$$

which can be calculated numerically by solving the quantum master equation in Lindblad form or analytically by expanding the wave function of the system in the bare basis as

$$|\psi(t)\rangle = \sum_{\nu=0}^{2}\sum_{n=0}^{2} c_{\nu,n}|\nu, n\rangle, \tag{E2}$$

where $P_{\nu,n} = |c_{\nu,n}|^2$ is the population of the corresponding state $|\nu, n\rangle$. We truncate the expansion at $\nu_{\max} = 2$ and $n_{\max} = 2$, considering these levels as the last bare states populated in the dynamics. Thus, the equal-time second-order correlation function in equation (E3) is approximately given by

$$g^{(2)}(0) = \frac{2(P_{0,2} + P_{1,2} + P_{2,2})}{[P_{0,1} + P_{1,1} + P_{2,1} + 2(P_{0,2} + P_{1,2} + P_{2,2})]^2}. \tag{E3}$$

Figure E.1 shows the equal-time correlation function in equation (E3) as a function of time when the laser pulse is active. In this time interval ($300 < t < 900$ fs), $g^{(2)}(0)$ has values smaller than one for $F_0/\kappa = 0.2$ (blue line), which indicates a photon blockade effect in contrast with the weak driving scenario $F_0/\kappa = 0.01$ (black line). Although the reduction of the equal-time second order correlation function is small, it is sufficient to generate a power-dependent time delay in the FID signal.

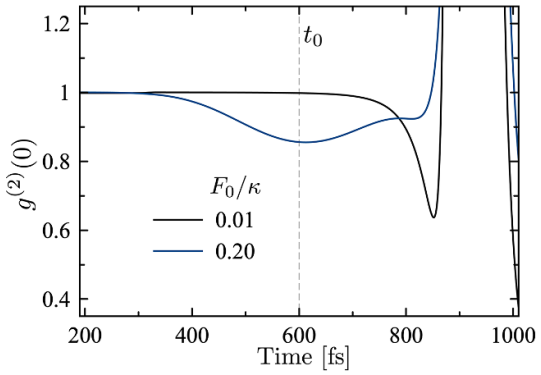

Figure E.1. Equal-time second order correlation function. $g^{(2)}(0)$ function as function of time for laser intensities $F_0 = 0.01\kappa$ and $F_0 = 0.20\kappa$ by solving the Lindblad quantum master equation for $U/\gamma_1 = 1.0$ (scenario shows in figure 2). Additional parameters for all panels are $\{\omega_0, \kappa, \gamma_1, \sqrt{N}g\} = \{40.0, 12.0, 0.6, 1.0\}$ THz.

ORCID iDs

Mauricio Arias https://orcid.org/0009-0001-0347-782X
Johan F Triana https://orcid.org/0000-0001-9551-3121
Aldo Delgado https://orcid.org/0000-0002-8968-5733
Felipe Herrera https://orcid.org/0000-0001-8121-1931

References

[1] Haroche S, Brune M and Raimond J M 2020 *Nat. Phys.* **16** 243
[2] O'Brien J L, Furusawa A and Vučković J 2009 *Nat. Photon.* **3** 687
[3] Kimble H J 1998 *Phys. Scr.* **1998** 127
[4] Ruddell S K, Webb K E, Herrera I, Parkins A S and Hoogerland M D 2017 *Optica* **4** 576
[5] Mabuchi H and Doherty A C 2002 *Science* **298** 1372
[6] Vahala K J 2003 *Nature* **424** 839
[7] Ballarini D and De Liberato S 2019 *Nanophotonics* **8** 641
[8] Kiraz A, Reese C, Gayral B, Zhang L, Schoenfeld W V, Gerardot B D, Petroff P M, Hu E L and Imamoğlu A 2003 *J. Opt. B: Quantum Semiclass. Opt.* **5** 129
[9] Blais A, Huang R-S, Wallraff A, Girvin S M and Schoelkopf R J 2004 *Phys. Rev.* A **69** 062320
[10] Fink J M, Göppl M, Baur M, Bianchetti R, Leek P J, Blais A and Wallraff A 2008 *Nature* **454** 315
[11] Putz S, Krimer D O, Amsüss R, Valookaran A, Nöbauer T, Schmiedmayer J, Rotter S and Majer J 2014 *Nat. Phys.* **10** 720
[12] Reagor M *et al* 2016 *Phys. Rev.* B **94** 014506
[13] Blais A, Girvin S M and Oliver W D 2020 *Nat. Phys.* **16** 247
[14] Dini D, Köhler R, Tredicucci A, Biasiol G and Sorba L 2003 *Phys. Rev. Lett.* **90** 116401
[15] Günter G *et al* 2009 *Nature* **458** 178
[16] Mann S A, Nookala N, Johnson S C, Cotrufo M, Mekawy A, Klem J F, Brener I, Raschke M B, Alù A and Belkin M A 2021 *Optica* **8** 606
[17] Paul P, Addamane S J and Liu P Q 2023 *Nano Lett.* **23** 2890
[18] Long J P and Simpkins B S 2015 *ACS Photonics* **2** 130
[19] Dunkelberger A D, Spann B T, Fears K P, Simpkins B S and Owrutsky J C 2016 *Nat. Commun.* **7** 1
[20] Xiang B, Ribeiro R F, Li Y, Dunkelberger A D, Simpkins B B, Yuen-Zhou J and Xiong W 2019 *Sci. Adv.* **5** aax5196
[21] George J, Chervy T, Shalabney A, Devaux E, Hiura H, Genet C and Ebbesen T W 2016 *Phys. Rev. Lett.* **117** 153601
[22] George J, Shalabney A, Hutchison J A, Genet C and Ebbesen T W 2015 *J. Phys. Chem. Lett.* **6** 1027
[23] Shalabney A, George J, Hutchison J, Pupillo G, Genet C and Ebbesen T W 2015 *Nat. Commun.* **6** 1
[24] Vigneron P-B, Pirotta S, Carusotto I, Tran N-L, Biasiol G, Manceau J-M, Bousseksou A and Colombelli R 2019 *Appl. Phys. Lett.* **114** 131104
[25] Nagarajan K, Thomas A and Ebbesen T W 2021 *J. Am. Chem. Soc.* **143** 16877
[26] Ahn W, Triana J F, Recabal F, Herrera F and Simpkins B S 2023 *Science* **380** 1165
[27] Milonni P W and Knight P L 1973 *Opt. Commun.* **9** 119
[28] Barnes W L 1998 *J. Mod. Opt.* **45** 661
[29] Akselrod G M, Argyropoulos C, Hoang T B, Ciracì C, Fang C, Huang J, Smith D R and Mikkelsen M H 2014 *Nat. Photon.* **8** 835
[30] Harrington P M, Mueller E J and Murch K W 2022 *Nat. Rev. Phys.* **4** 660
[31] Jacob Z, Smolyaninov I I and Narimanov E E 2012 *Appl. Phys. Lett.* **100** 181105
[32] Genes C, Vitali D, Tombesi P, Gigan S and Aspelmeyer M 2008 *Phys. Rev.* A **77** 033804
[33] Carlon Zambon N, Denis Z, De Oliveira R, Ravets S, Ciuti C, Favero I and Bloch J 2022 *Phys. Rev. Lett.* **129** 093603
[34] Petiziol F and Eckardt A 2022 *Phys. Rev. Lett.* **129** 233601
[35] Nishida J, Johnson S C, Chang P T S, Wharton D M, Dönges S A, Khatib O and Raschke M B 2022 *Nat. Commun.* **13** 1083
[36] Triana J F, Arias M, Nishida J, Muller E A, Wilcken R, Johnson S C, Delgado A, Raschke M B and Herrera F 2022 *J. Chem. Phys.* **156** 124110
[37] Metzger B, Muller E, Nishida J, Pollard B, Hentschel M and Raschke M B 2019 *Phys. Rev. Lett.* **123** 153001

[38] Vilas N B, Hallas C, Anderegg L, Robichaud P, Zhang C, Dawley S, Cheng L and Doyle J M 2023 *Phys. Rev.* A **107** 062802
[39] Lyubomirsky I, Hu Q and Melloch M R 1998 *Appl. Phys. Lett.* **73** 3043
[40] Wilcken R, Nishida J, Triana J F, John-Herpin A, Altug H, Sharma S, Herrera F and Raschke M B 2023 *Proc. Natl Acad. Sci.* **120** e2220852120
[41] Golonzka O, Khalil M, Demirdöven N and Tokmakoff A 2001 *Phys. Rev. Lett.* **86** 2154
[42] Anfuso C L, Ricks A M, Rodríguez-Córdoba W and Lian T 2012 *J. Phys. Chem.* C **116** 26377
[43] Zubairy M S, Kim M and Scully M O 2003 *Phys. Rev.* A **68** 033820
[44] Duan L-M and Kimble H J 2004 *Phys. Rev. Lett.* **92** 127902
[45] van Enk S J, Kimble H J and Mabuchi H 2004 *Quantum Inf. Process.* **3** 75
[46] Turchette Q A, Hood C J, Lange W, Mabuchi H and Kimble H J 1995 *Phys. Rev. Lett.* **75** 4710
[47] Tiecke T G, Thompson J D, de Leon N P, Liu L R, Vuletić V and Lukin M D 2014 *Nature* **508** 241
[48] Young A B *et al* 2011 *Phys. Rev.* A **84** 011803
[49] Hughes S and Roy C 2012 *Phys. Rev.* B **85** 035315
[50] Ho S T, Soccolich C E, Islam M N, Hobson W S, Levi A F J and Slusher R E 1991 *Appl. Phys. Lett.* **59** 2558
[51] Axt V M and Mukamel S 1998 *Rev. Mod. Phys.* **70** 145
[52] Faraon A, Majumdar A and Vučković J 2010 *Phys. Rev.* A **81** 033838
[53] Birnbaum K M, Boca A, Miller R, Boozer A D, Northup T E and Kimble H J 2005 *Nature* **436** 87
[54] Xiang B, Ribeiro R F, Dunkelberger A D, Wang J, Li Y, Simpkins B S, Owrutsky J C, Yuen-Zhou J and Xiong W 2018 *Proc. Natl Acad. Sci.* **115** 4845
[55] Herrera F and Owrutsky J 2020 *J. Chem. Phys.* **152** 100902
[56] Grafton A B, Dunkelberger A D, Simpkins B S, Triana J F, Hernández F J, Herrera F and Owrutsky J C 2021 *Nat. Commun.* **12** 214
[57] Kadyan A, Shaji A and George J 2021 *J. Phys. Chem. Lett.* **12** 4313
[58] Wright A D, Nelson J C and Weichman M L 2023 *J. Am. Chem. Soc.* **145** 5982
[59] Menghrajani K S, Chen M, Dholakia K and Barnes W L 2022 *Ad. Opt. Mater.* **10** 2102065
[60] Zaks B, Stehr D, Truong T-A, Petroff P M, Hughes S and Sherwin M S 2011 *New J. Phys.* **13** 083009
[61] Autore M *et al* 2018 *Light: Sci. Appl.* **7** 17172
[62] Bylinkin A *et al* 2021 *Nat. Photon.* **15** 197
[63] Muller E A, Pollard B, Bechtel H A, Adato R, Etezadi D, Altug H and Raschke M B 2018 *ACS Photonics* **5** 3594
[64] Xu X G and Raschke M B 2013 *Nano Lett.* **13** 1588
[65] Pollard B, Muller E A, Hinrichs K and Raschke M B 2014 *Nat. Commun.* **5** 3587
[66] Autore M *et al* 2021 *Adv. Opt. Mater.* **9** 2001958
[67] Huth F, Chuvilin A, Schnell M, Amenabar I, Krutokhvostov R, Lopatin S and Hillenbrand R 2013 *Nano Lett.* **13** 1065
[68] Miller D 1997 Optical physics of quantum wells *Quantum Dynamics of Simple Systems* 1st edn (Taylor & Francis) pp 239–66
[69] Goulain P, Deimert C, Jeannin M, Pirotta S, Pasek W J, Wasilewski Z, Colombelli R and Manceau J-M 2023 *Adv. Opt. Mater.* **11** 2202724
[70] Fulmer E C, Mukherjee P, Krummel A T and Zanni M T 2004 *J. Chem. Phys.* **120** 8067
[71] Dunkelberger A D, Grafton A B, Vurgaftman I, Soykal O O, Reinecke T L, Davidson R B, Simpkins B S and Owrutsky J C 2019 *ACS Photonics* **6** 2719
[72] Levine B F 1993 *J. Appl. Phys.* **74** R1
[73] Mann S A, Nookala N, Johnson S, Mekkawy A, Klem J F, Brener I, Raschke M, Alù A and Belkin M A 2020 *Conf. on Lasers and Electro-Optics* (Optical Society of America) p FTu4Q.7
[74] Plankensteiner D, Sommer C, Reitz M, Ritsch H and Genes C 2019 *Phys. Rev.* A **99** 043843
[75] Német N, White D, Kato S, Parkins S and Aoki T 2020 *Phys. Rev. Appl.* **13** 064010
[76] Carmichael H 1999 *Statistical Methods in Quantum Optics 1: Master Equations and Fokker-Planck Equations* (*Physics and Astronomy Online Library*) (Springer)
[77] Johansson J, Nation P and Nori F 2012 *Comput. Phys. Commun.* **183** 1760
[78] Johansson J, Nation P and Nori F 2013 *Comput. Phys. Commun.* **184** 1234
[79] Zou F, Lai D-G and Liao J-Q 2020 *Opt. Express* **28** 16175
[80] Benea-Chelmus I-C, Settembrini F F, Scalari G and Faist J 2019 *Nature* **568** 202
[81] De Liberato S 2019 *Phys. Rev.* A **100** 031801
[82] Wang Y and De Liberato S 2021 *Phys. Rev.* A **104** 023109
[83] Kizmann M, Moskalenko A S, Leitenstorfer A, Burkard G and Mukamel S 2022 *Laser Photon. Rev.* **16** 2100423
[84] Waks E, Diamanti E, Sanders B C, Bartlett S D and Yamamoto Y 2004 *Phys. Rev. Lett.* **92** 113602
[85] Zhu D *et al* 2022 *Light: Sci. Appl.* **11** 327
[86] Shammah N, Lambert N, Nori F and De Liberato S 2017 *Phys. Rev.* A **96** 023863
[87] Manzano D 2020 *AIP Adv.* **10** 025106
[88] Stuart J T 1958 *J. Fluid Mech.* **4** 1
[89] Panteley E, Loria A and Ati A E 2015 *IFAC-PapersOnLine* **48** 645